# Supplementary Materials: Air Quality in the Italian Northwestern Alps during Year 2020: Assessment of the COVID-19 «Lockdown Effect» from Multi-Technique Observations and Models

**Henri Diémoz, Tiziana Magri, Giordano Pession, Claudia Tarricone, Ivan Karl Friedrich Tombolato, Gabriele Fasano, and Manuela Zublena**

## S1. Validation of the predictive statistical model (random forest)

As mentioned in the main text, several models are trained for validation purposes over five periods (of 5 years each), i.e. 2010–2014, 2011–2015, 2012–2016, 2013–2017, 2014–2018, and they are compared with real measurements from years 2015, 2016, 2017, 2018, and 2019, respectively. Here we report the mean bias (MB) and the Pearson's correlation coefficient (R), as metrics of the model reliability.

**Table S1.** Comparison metrics between measurements and predictions by the statistical model for NO.

| Year | Training period | Courmayeur | | Aosta–downtown | | Donnas | |
|---|---|---|---|---|---|---|---|
| | | **MB** ($\mu g\ m^{-3}$) | **R** | **MB** ($\mu g\ m^{-3}$) | **R** | **MB** ($\mu g\ m^{-3}$) | **R** |
| 2015 | 2010–2014 | 5.8 | 0.8 | 4.1 | 0.9 | 1.9 | 0.7 |
| 2016 | 2011–2015 | 0.2 | 0.7 | 10.4 | 0.9 | 2.6 | 0.7 |
| 2017 | 2012-2016 | 8.8 | 0.8 | 1.8 | 0.9 | 2.4 | 0.6 |
| 2018 | 2013–2017 | 8.5 | 0.7 | 13.1 | 0.8 | 1.4 | 0.7 |
| 2019 | 2014–2018 | 6.4 | 0.6 | 3.1 | 0.9 | 3.6 | 0.7 |

**Table S2.** Comparison metrics between measurements and predictions by the statistical model for $NO_2$.

| Year | Training period | Courmayeur | | Aosta–downtown | | Donnas | |
|---|---|---|---|---|---|---|---|
| | | **MB** ($\mu g\ m^{-3}$) | **R** | **MB** ($\mu g\ m^{-3}$) | **R** | **MB** ($\mu g\ m^{-3}$) | **R** |
| 2015 | 2010–2014 | 3.6 | 0.7 | 1.6 | 0.9 | 0.0 | 0.9 |
| 2016 | 2011–2015 | 1.2 | 0.8 | 2.3 | 0.9 | 2.4 | 0.9 |
| 2017 | 2012-2016 | 0.4 | 0.8 | -2.0 | 0.9 | 0.0 | 0.9 |
| 2018 | 2013–2017 | 8.6 | 0.6 | 5.8 | 0.9 | 3.7 | 0.8 |
| 2019 | 2014–2018 | 8.0 | 0.7 | 2.1 | 0.9 | 4.5 | 0.8 |

**Table S3.** Comparison metrics between measurements and predictions by the statistical model for $O_3$.

| Year | Training period | Aosta–downtown | | Donnas | |
|---|---|---|---|---|---|
| | | **MB** ($\mu g\ m^{-3}$) | **R** | **MB** ($\mu g\ m^{-3}$) | **R** |
| 2015 | 2010–2014 | -4.1 | 0.9 | -5.4 | 0.9 |
| 2016 | 2011–2015 | 0.5 | 0.9 | -7.1 | 0.9 |
| 2017 | 2012-2016 | -3.4 | 0.9 | -5.6 | 0.9 |
| 2018 | 2013–2017 | 0.6 | 0.9 | 5.5 | 0.9 |
| 2019 | 2014–2018 | 1.5 | 0.9 | -1.5 | 0.9 |

**Table S4.** Comparison metrics between measurements and predictions by the statistical model for $PM_{2.5}$.

| Year | Training period | Aosta–downtown | |
|---|---|---|---|
| | | **MB** ($\mu g\ m^{-3}$) | **R** |
| 2015 | 2010–2014 | 2.1 | 0.8 |
| 2016 | 2011–2015 | 2.1 | 0.8 |
| 2017 | 2012-2016 | -0.7 | 0.8 |
| 2018 | 2013–2017 | 3.5 | 0.7 |
| 2019 | 2014–2018 | 0.4 | 0.7 |

**Table S5.** Comparison metrics between measurements and predictions by the statistical model for $PM_{10}$.

| Year | Training period | Courmayeur | | Aosta–downtown | | Donnas | |
|---|---|---|---|---|---|---|---|
| | | **MB** ($\mu g\ m^{-3}$) | **R** | **MB** ($\mu g\ m^{-3}$) | **R** | **MB** ($\mu g\ m^{-3}$) | **R** |
| 2015 | 2010–2014 | 4.0 | 0.6 | 3.1 | 0.8 | -0.2 | 0.7 |
| 2016 | 2011–2015 | 1.6 | 0.6 | 4.4 | 0.8 | 1.4 | 0.7 |
| 2017 | 2012-2016 | 1.6 | 0.7 | -1.7 | 0.8 | 1.2 | 0.7 |
| 2018 | 2013–2017 | 5.1 | 0.4 | 4.1 | 0.7 | 7.5 | 0.7 |
| 2019 | 2014–2018 | 4.1 | 0.4 | 2.2 | 0.7 | 2.2 | 0.7 |

## S2. Details on the emission inventory and its variations in 2020

The 11 SNAP97 categories related to the types of local emission sources are listed in the following table, according to the European CORINAIR method (e.g., https://www.eea.europa.eu/publications/EMEPCORINAIR5, last access: 22 June 2021).

**Table S6.** The 11 SNAP97 categories defined by the European CORINAIR method.

| Category | Code |
|---|---|
| Combustion in energy and transformation industries | 01 |
| Non-industrial combustion plants | 02 |
| Combustion in manufacturing industry | 03 |
| Production processes | 04 |
| Extraction and distribution of fossil fuels and geothermal energy | 05 |
| Solvent and other product use | 06 |
| Road transport | 07 |
| Other mobile source and machinery | 08 |
| Waste treatment and disposal | 09 |
| Agriculture | 10 |
| Other sources and sinks | 11 |

## S3. Details on the meteorological context in 2020 compared to the previous years

The same weather classification introduced in one of our previous studies [1] was used here to easily compare the meteorological patterns in 2020 to the previous years.


**Figure S1.** Occurrence of different weather types in the analysed periods for different years. The month initials are reported in parentheses next to the period for better understanding. Notice the different range of the vertical scales in the subfigures.

We also show the statistical distributions of the daily average air temperature and the total precipitation in each period.

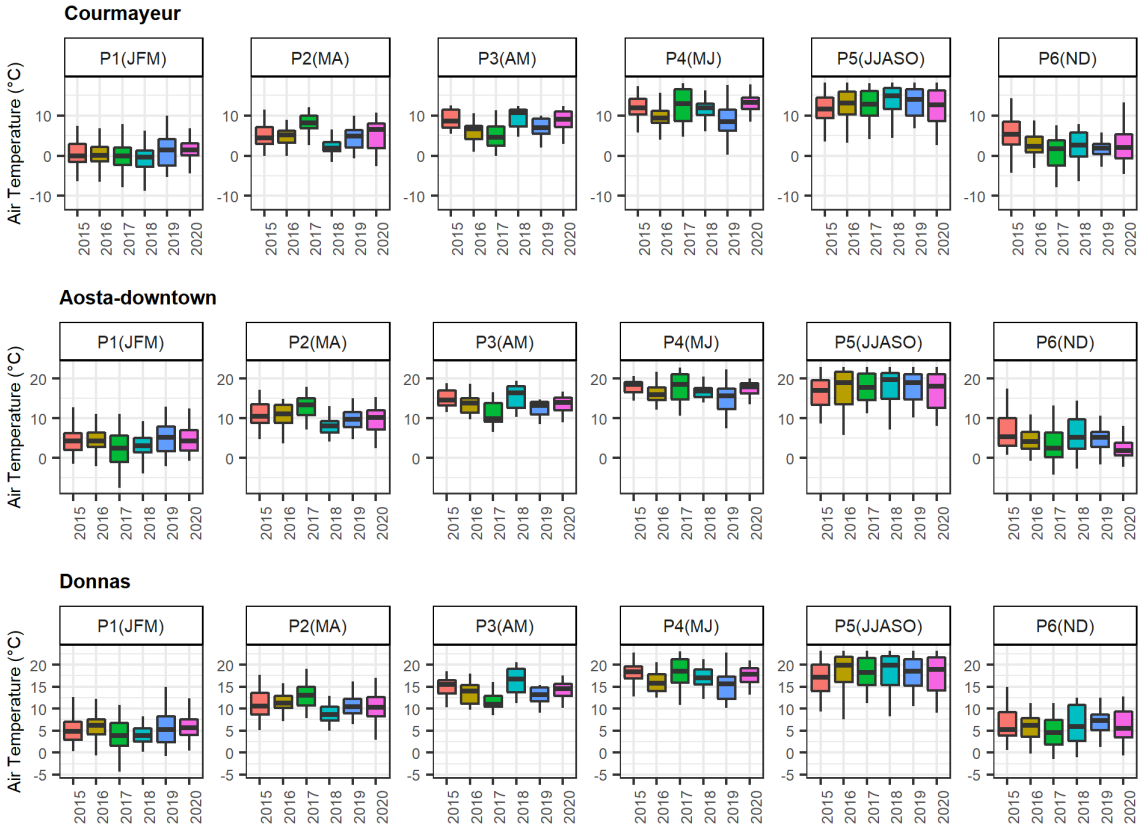


**Figure S2.** Comparison of daily average air temperature in the analysed periods for different years.

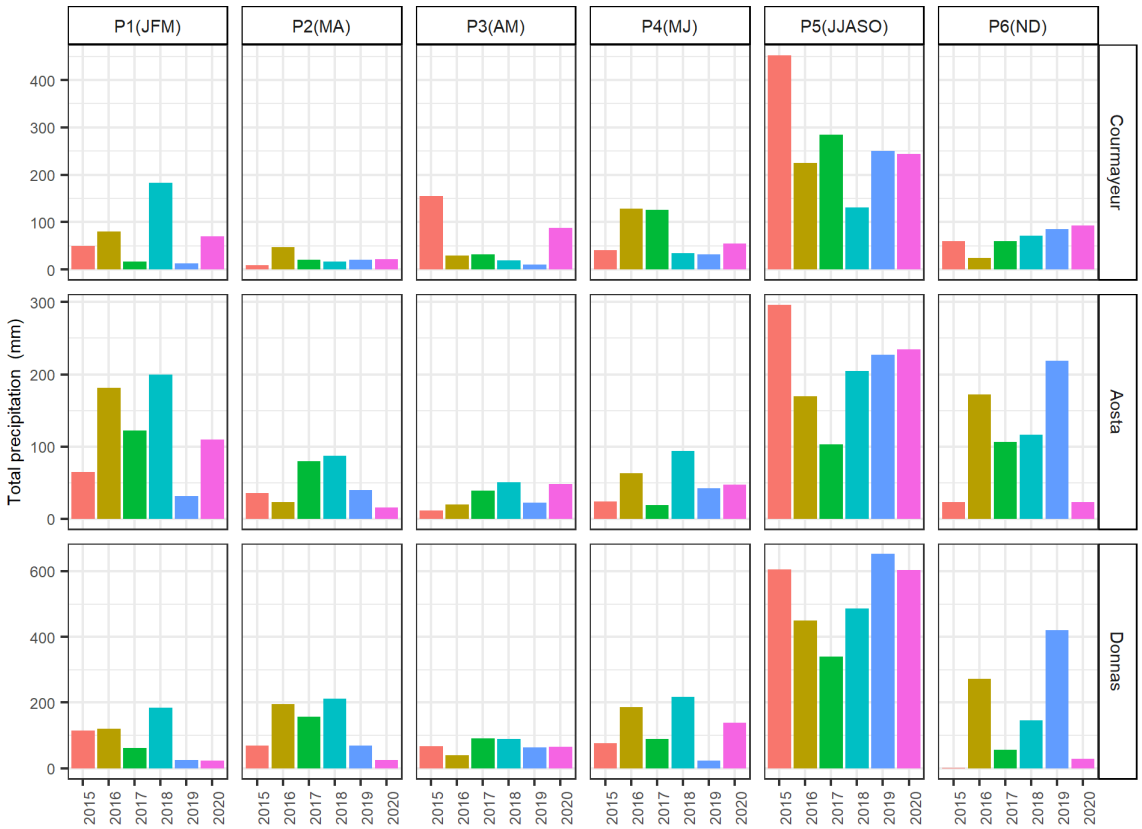


**Figure S3.** Comparison of total precipitation in the analysed periods for different years.

## S4. Details on changes in gaseous pollutant concentrations

The statistical distribution of the daily average concentrations of surface gaseous pollutants measured in the last six years at different air quality stations are show here below (the respective plot for $NO_2$ can be found in the main text).

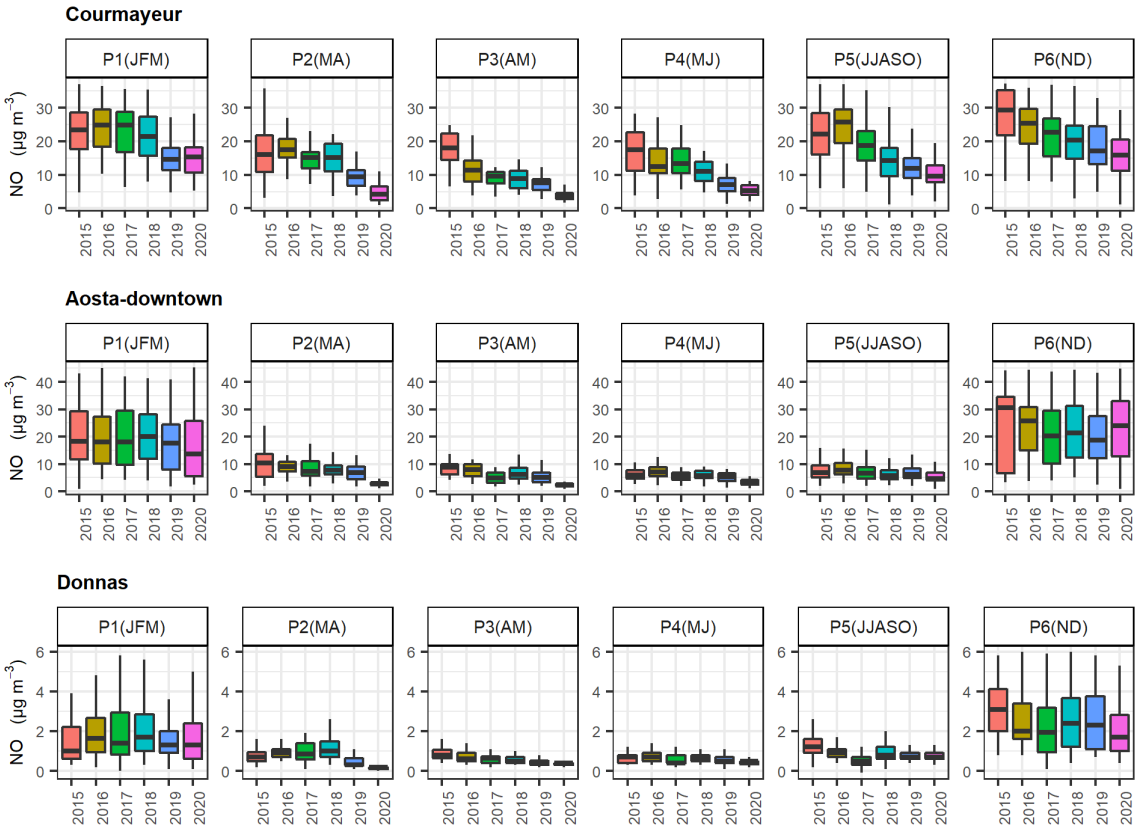


**Figure S4.** Median (horizontal line in the box), interquartile range (box height), overall variability excluding outliers (vertical line) of daily average NO concentrations measured in each period (cf. definitions in the main text) of the last 6 years at each air quality station. Notice that the ranges of the vertical scale at the three stations are different for better visualisation.

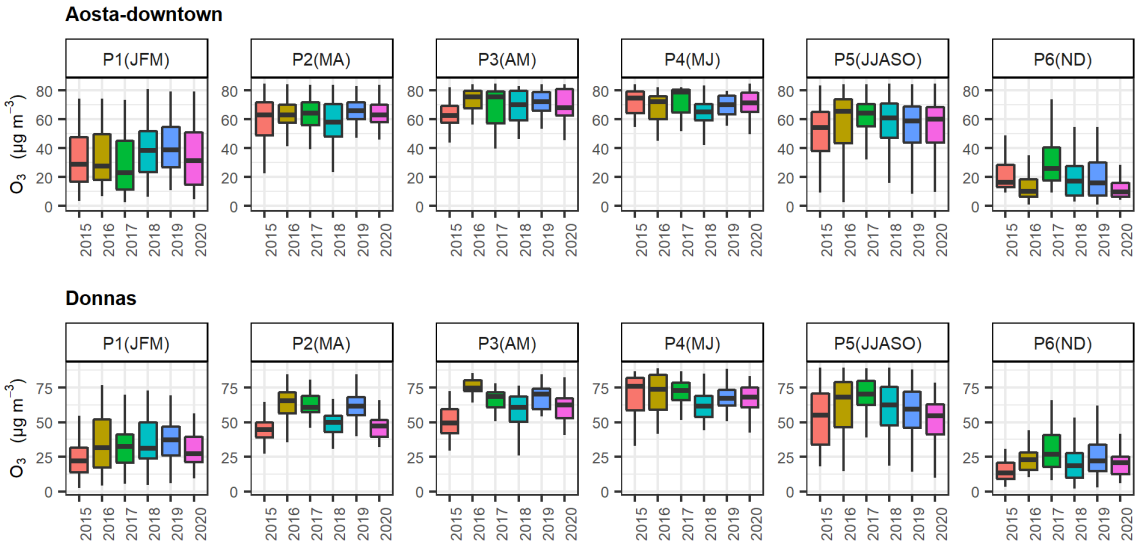


**Figure S5.** Same as the previous figure, for surface $O_3$ concentrations. Notice the different ranges of the vertical axes in the panels.

A comparison between actual observations and random forest forecasts (i.e., without considering changes in emissions) is show for each gaseous pollutant and each station here below. The respective plot for $NO_2$ can be found in the main text.

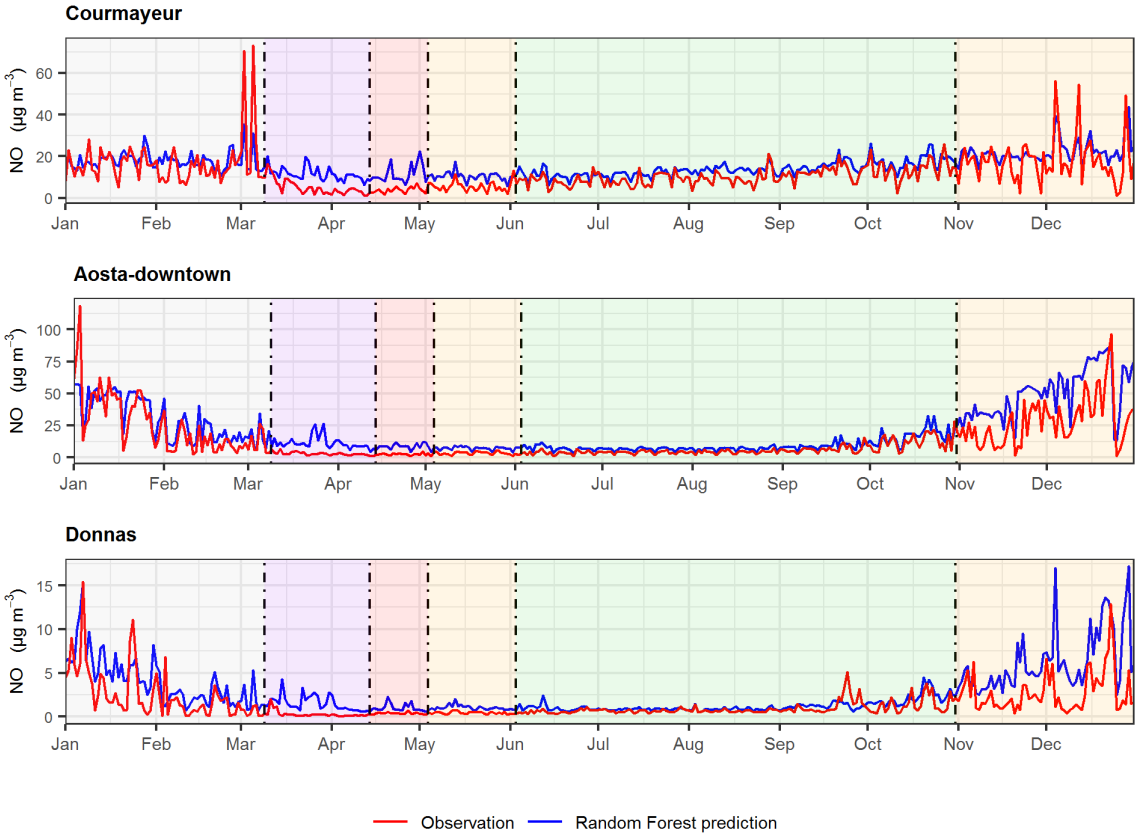


**Figure S6.** Observation (red) and prediction (blue) with the random forest algorithm of NO surface concentrations for year 2020. The vertical scales are different for ease of visualisation.

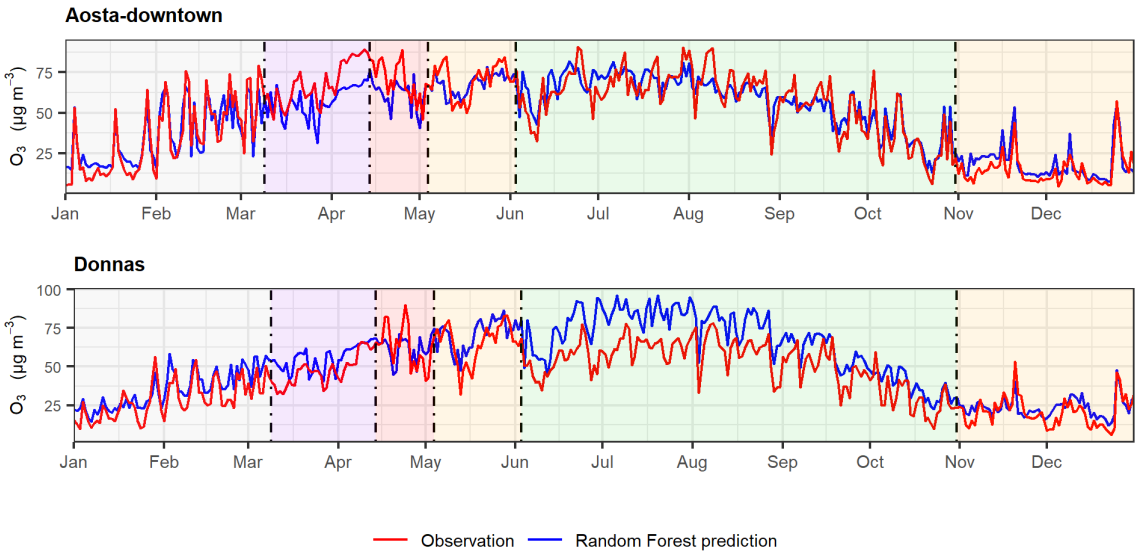


**Figure S7.** Observation (red) and prediction (blue) with the random forest algorithm of $O_3$ surface concentrations for year 2020. The vertical scales are different for ease of visualisation.

## S5. Details on changes in PM concentrations

The following plots represents the statistical distribution of daily average PM concentrations measured in the last six years at different air quality stations.

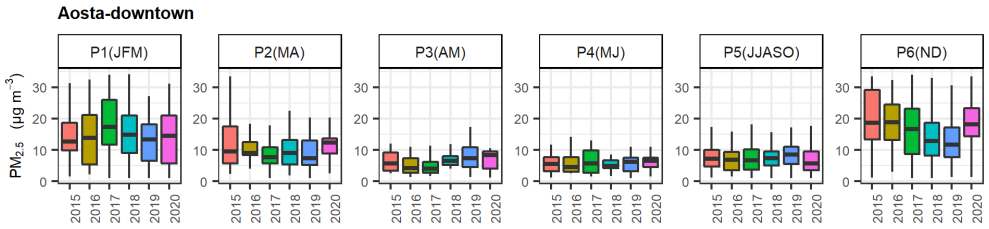


**Figure S8.** Median (horizontal line in the box), interquartile range (box height), overall variability (excluding outliers) of daily average $PM_{2.5}$ concentrations measured in each period (cf. definitions in the main text) of the last 6 years at each air quality station.

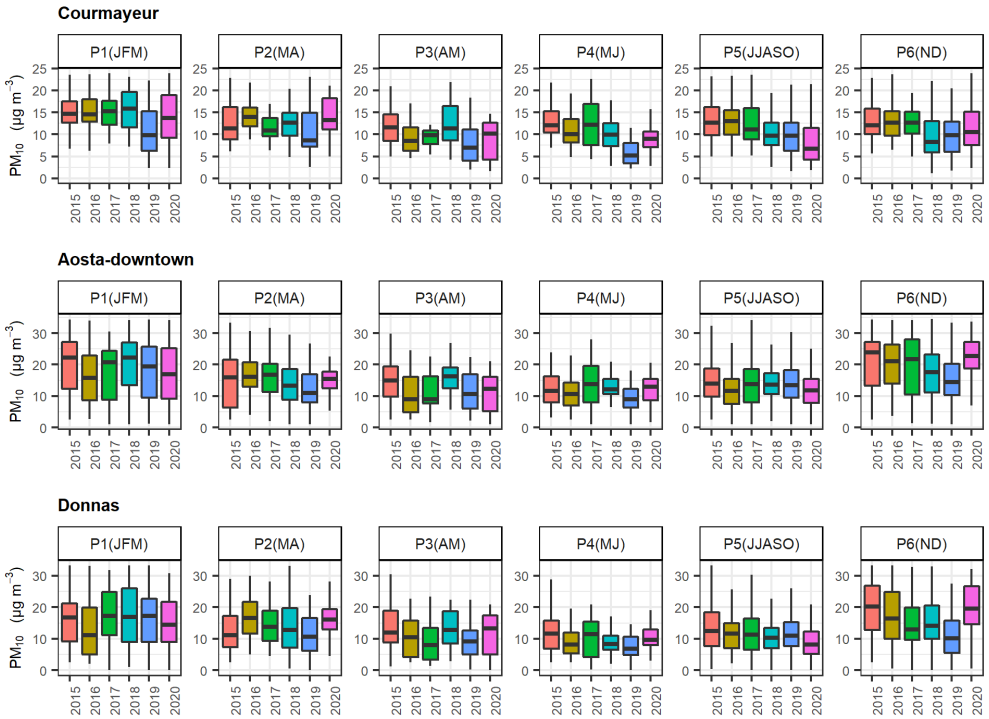


**Figure S9.** Same as the previous figure for surface $PM_{10}$ concentrations. Notice the difference in the range of the vertical axes.

Here below we represent the actual observations and the random forest forecasts for PM.

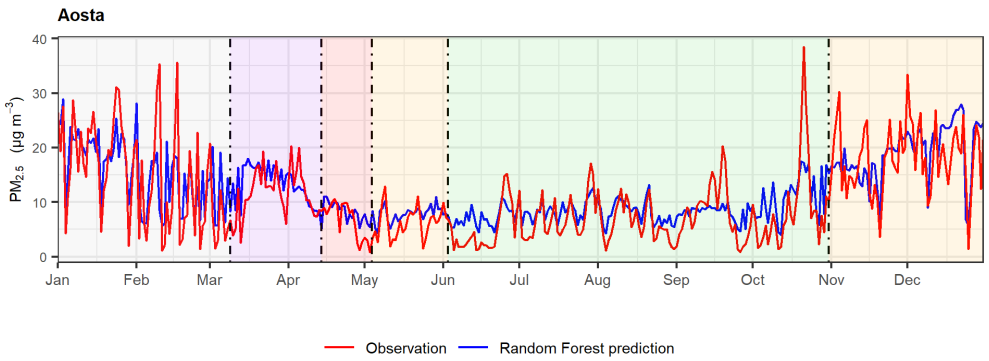


**Figure S10.** Observation (red) and prediction (blue) with the random forest algorithm of $PM_{2.5}$ surface concentrations in Aosta–downtown for year 2020.

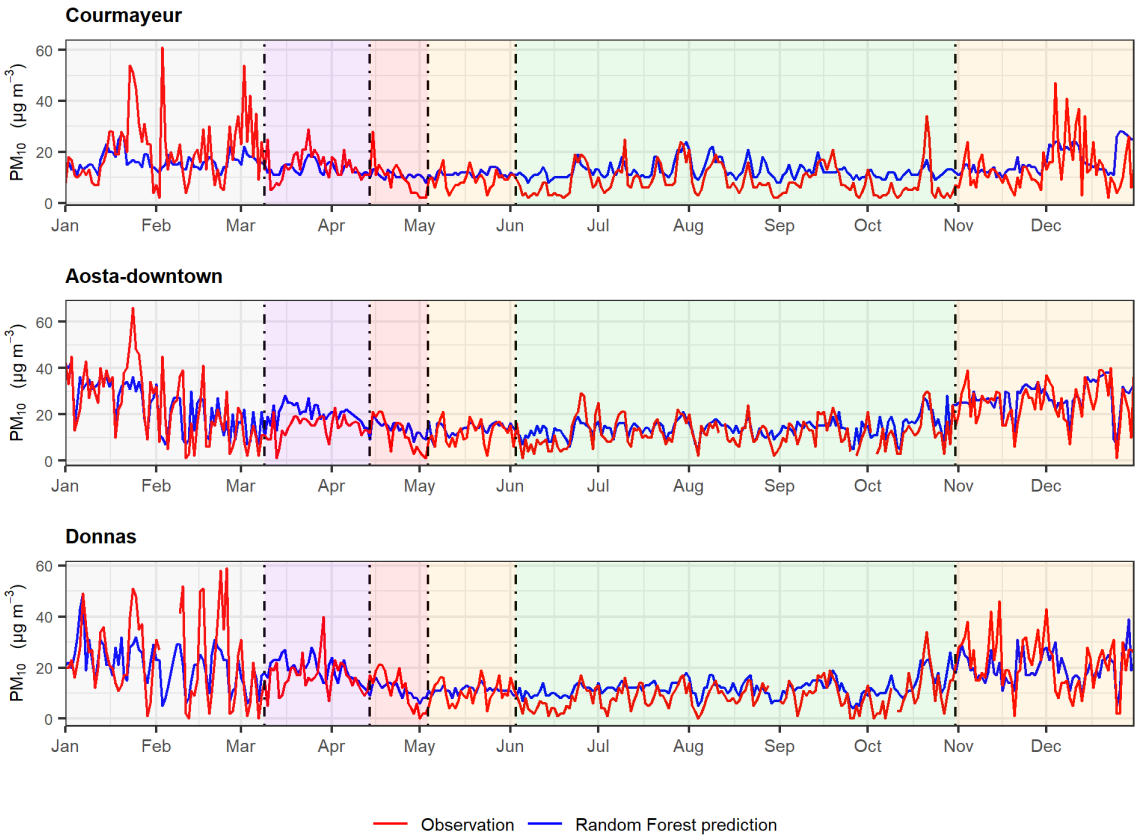


**Figure S11.** Observation (red) and prediction (blue) with the random forest algorithm of $PM_{10}$ surface concentrations at the different air quality stations for year 2020.

Total reductions in emissions of particulate matter from the inventory, resulting from curtailed emissions sources, are shown in the plot below.

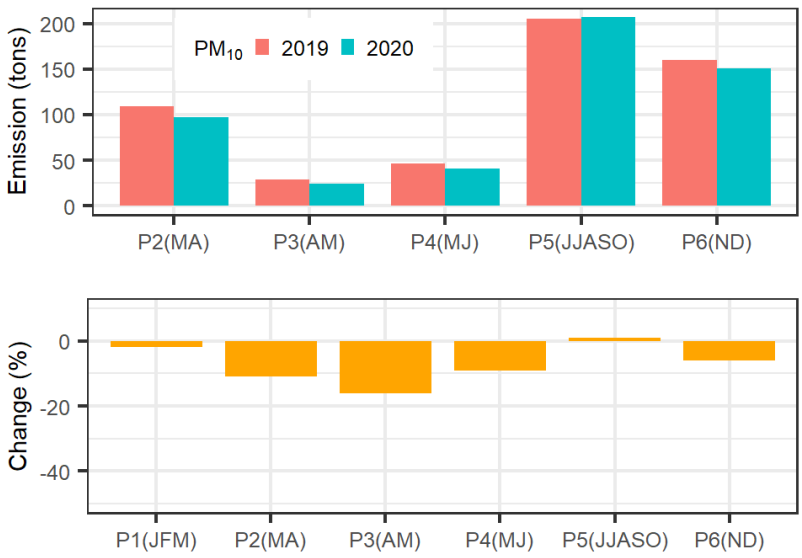


**Figure S12.** Total $PM_{10}$ emissions in the reference and curtailed scenarios and their percentage reduction over the domain of study. P1 is left unchanged, since it is prior to the lockdown measures. A similar figure for $NO_x$ is provided in the main text.

## S6. Details on aerosol source apportionment

The following plots represent the source profiles from size-PMF at each site where a Fidas200E Palas is installed.

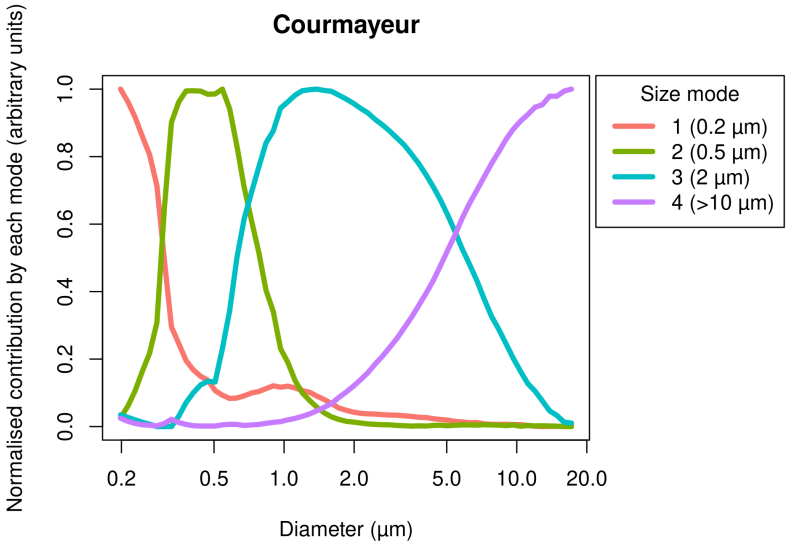


**Figure S13.** Modes resulting from size-PMF factorisation at Courmayeur in 2018–2020.

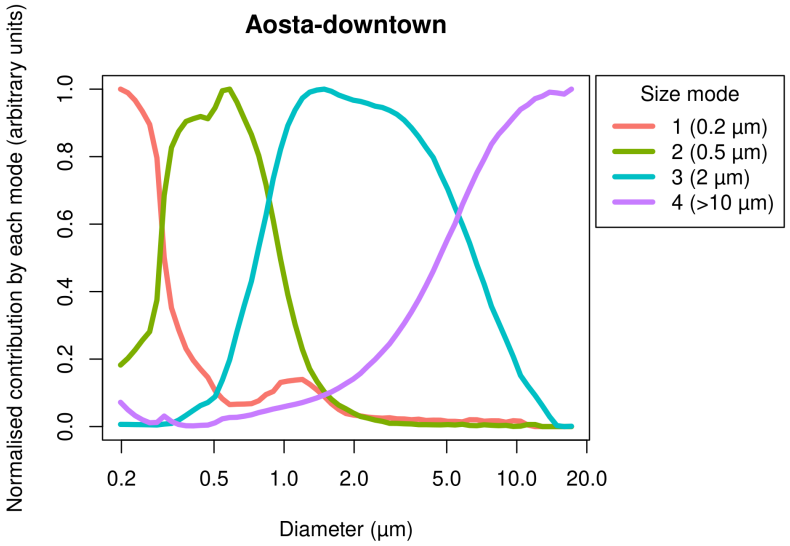


**Figure S14.** Modes resulting from the size-PMF factorisation at the Aosta–downtown station in 2019–2020.

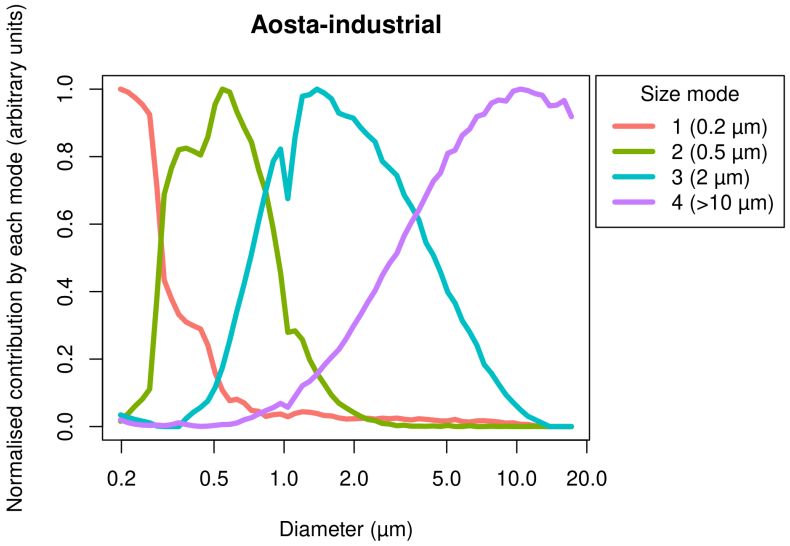


**Figure S15.** Modes resulting from the size-PMF factorisation at the Aosta–industrial station in 2019–2020.

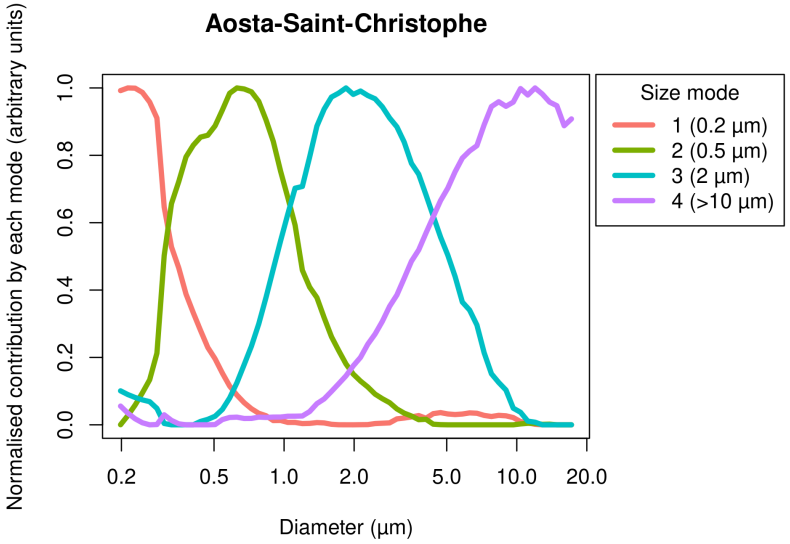


**Figure S16.** Modes resulting from the size-PMF factorisation at Aosta–Saint-Christophe in 2017–2019.

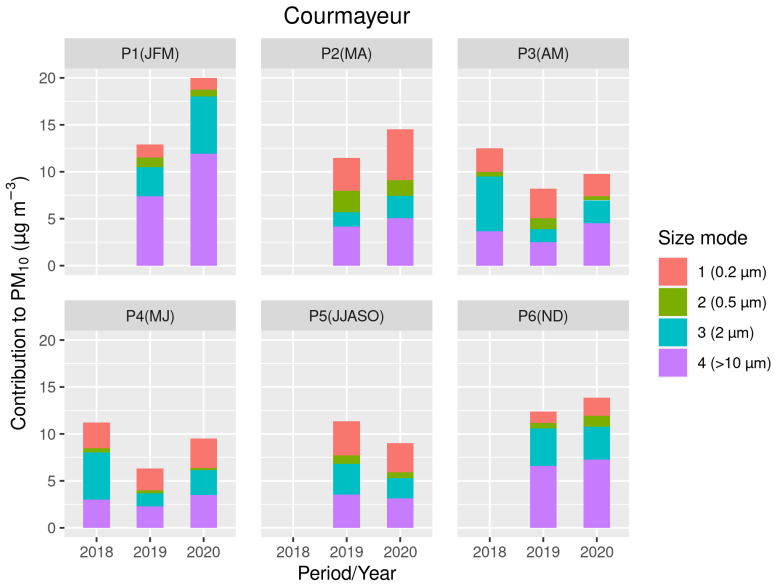


**Figure S17.** Contribution to the $PM_{10}$ concentration measured at the Courmayeur station by the four modes identified with size-PMF. Only periods with full data coverage are shown in the plot.

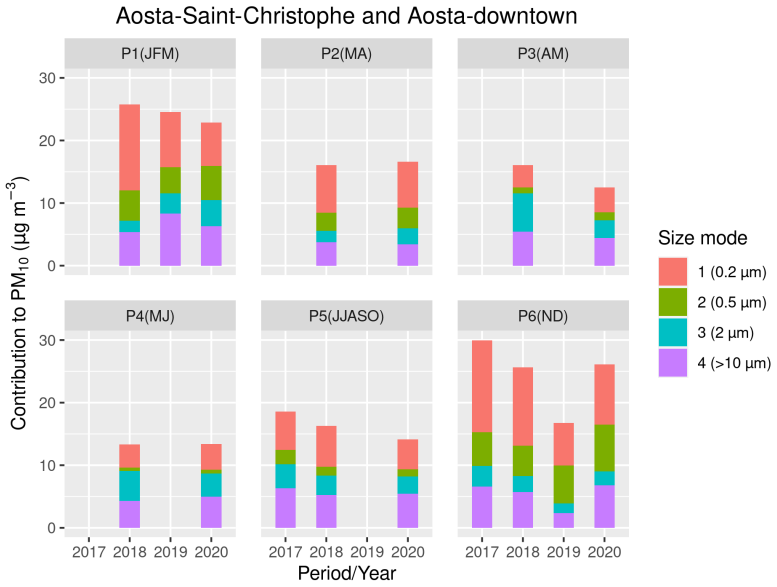


**Figure S18.** Same as the previous figure for the composite series from Aosta–Saint-Christophe (une 2017–March 2019) and Aosta–downtown (September 2019–2020).

The next figures show the source profiles from chem-PMF in Aosta–downtown using two different factorisations, one based on anion/cations and EC/OC/levoglucosan, and the other based on anion/cation plus metals.

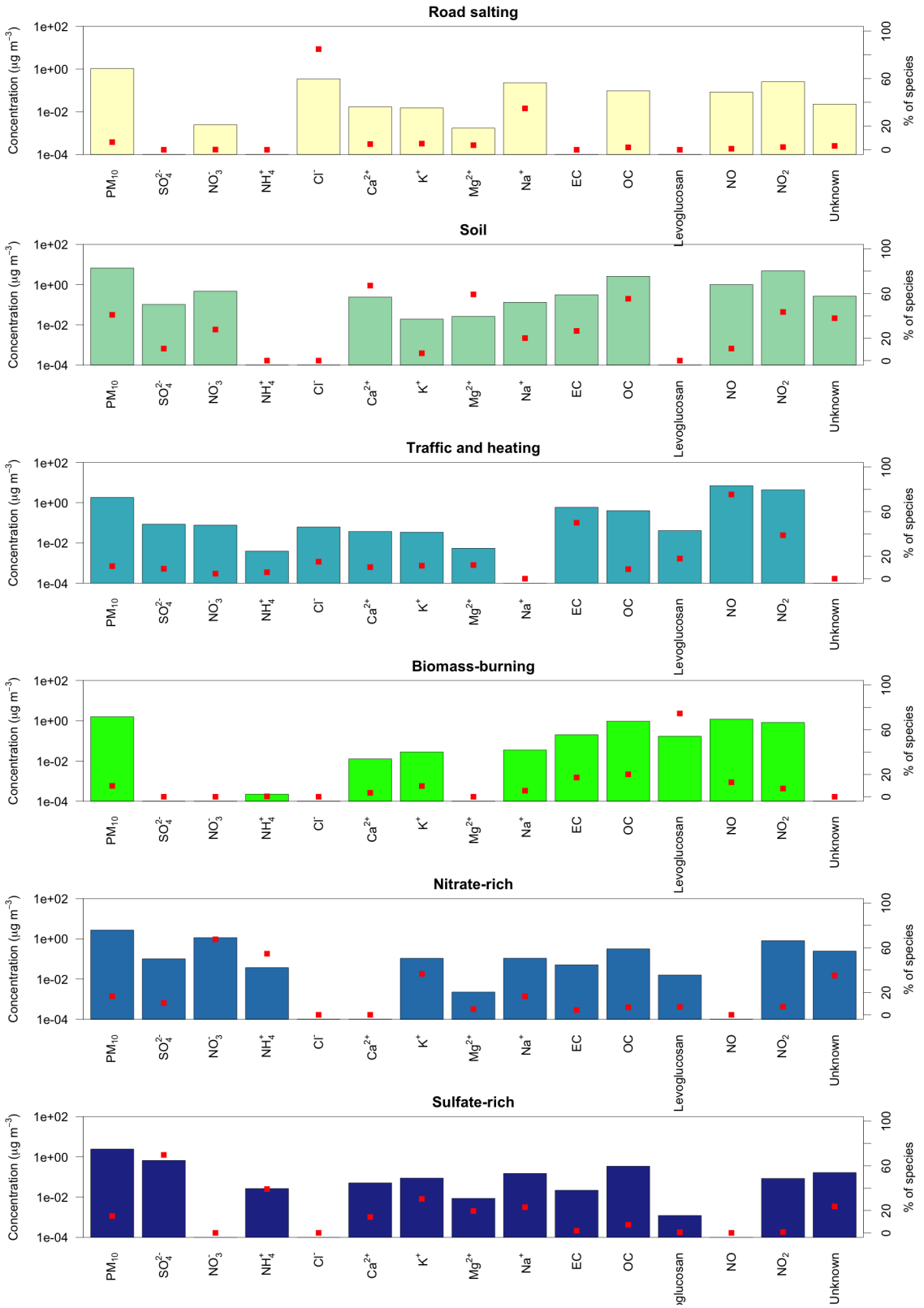


**Figure S19.** Factor profiles emerging from the anion/cation + EC/OC/levoglucosan chem-PMF. Coloured bars (left axis) represent absolute concentrations, red points (right axis) mark the percentage contribution to each mode of the total for each species.

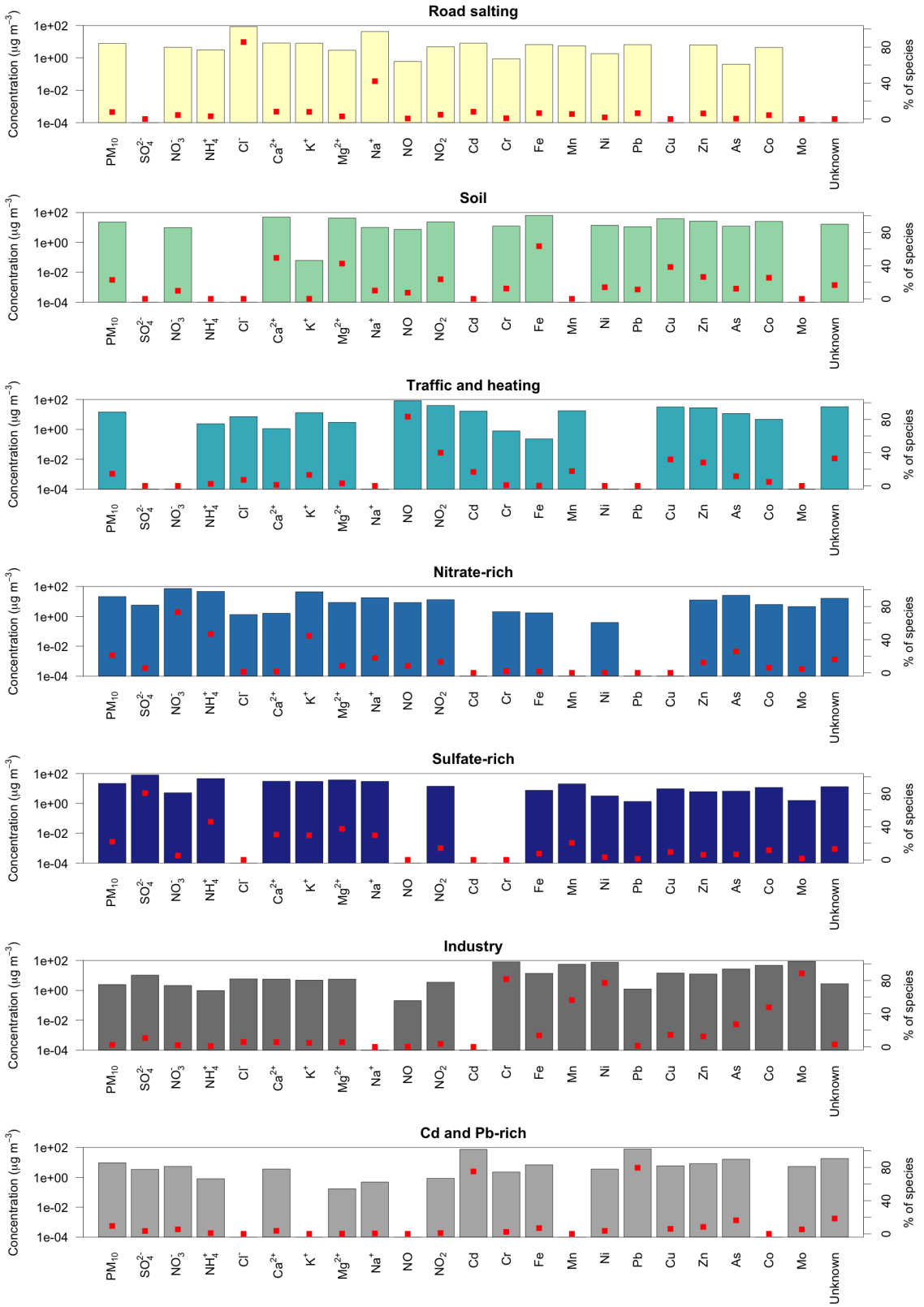


**Figure S20.** Factor profiles emerging from the anion/cation + metal chem-PMF.

The next figure shows the relative contribution of the biomass burning factor to the $PM_{2.5}$ mass concentration in Aosta–downtown.

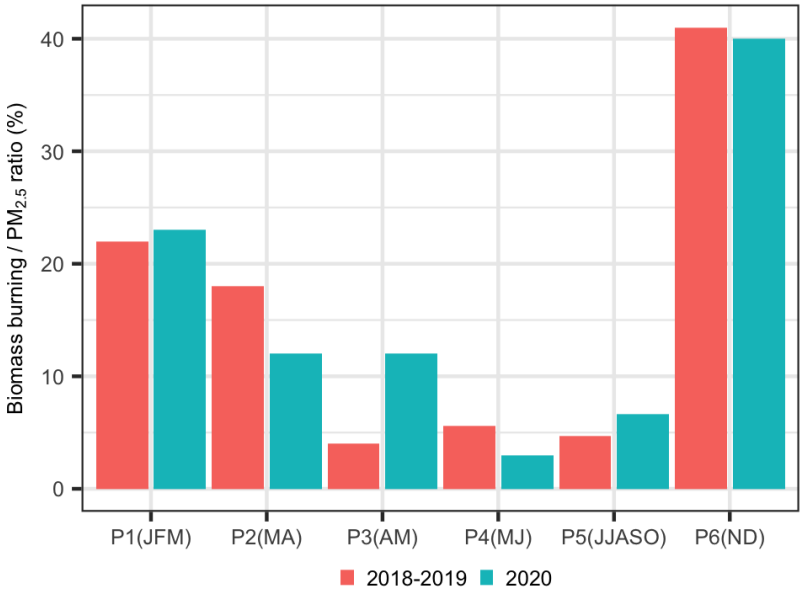


**Figure S21.** Contribution of the "biomass burning" mode to the $PM_{10}$ concentration in Aosta–downtown from chem-PMF based on anion/cation, EC/OC, and levoglucosan, further normalised using the total $PM_{2.5}$ concentration.

We report here below the estimates of eBC concentrations from the aethalometer data and their optical source apportionment.

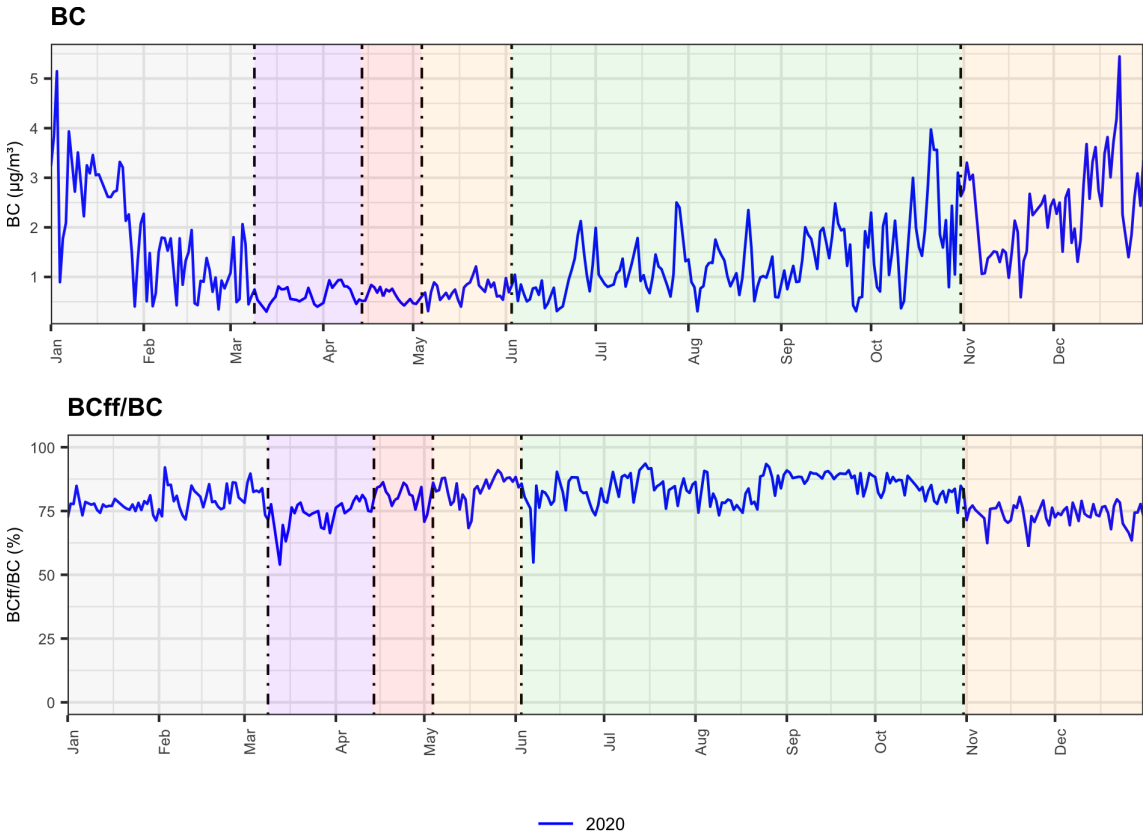


**Figure S22.** Absolute eBC concentrations measured in Aosta–downtown during 2020 and ratio between the fraction attributed to fossil fuel and total BC.

## S7. Results from the sun/sky radiometer

The variations, compared to the average over the previous years, of the aerosol optical depth (AOD) measured at a wavelength of 500 nm by the sun/sky radiometer are shown here below.

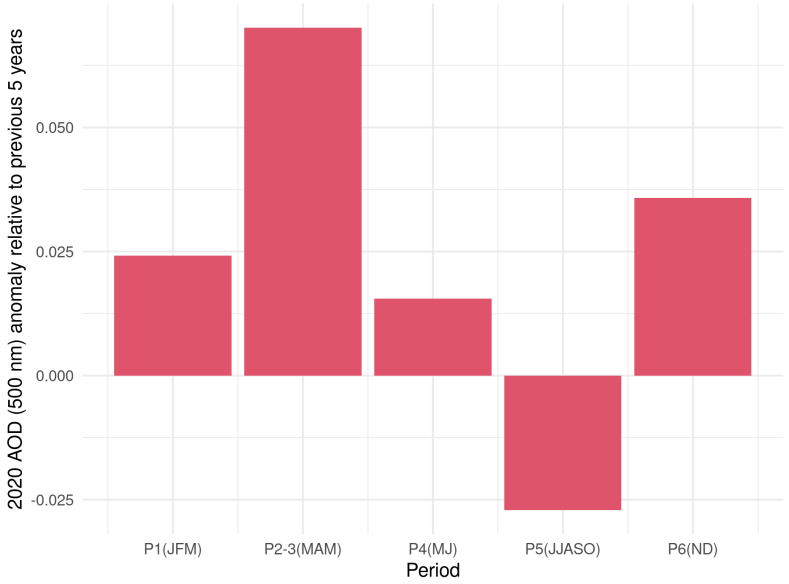


**Figure S23.** Aerosol optical depth (at 500 nm) absolute anomaly compared to the previous years, as measured by the POM-02 sun/sky radiometer.

## References

1. Diémoz, H.; Gobbi, G.P.; Magri, T.; Pession, G.; Pittavino, S.; Tombolato, I.K.F.; Campanelli, M.; Barnaba, F. Transport of Po Valley aerosol pollution to the northwestern Alps – Part 2: Long-term impact on air quality. *Atmos. Chem. Phys.* **2019**, *19*, 10129–10160. doi:10.5194/acp-19-10129-2019.